

PACS numbers: 42.25.Fx; 42.55.Rz; 81.05.Je
DOI: 10.1070/QE2014v044n06ABEH015454

Measurement of energy spectra of small-angle scattering and distribution of optical microinhomogeneities in laser ceramics

P.E. Tverdokhleb, Yu.A. Shepetkin, I.Sh. Steinberg, S.M. Vatnik, A.Yu. Belikov, I.A. Vedin, P.F. Kurbatov

Abstract. **The energy spectra of small-angle light scattering from the samples of Nd:YAG ceramics and the spatial distributions of optical microinhomogeneities in them are measured. The spatial profiles of microinhomogeneities are found using the collinear heterodyne microprobe technique. Based on the obtained data, the comparison of noise and lasing characteristics of foreign and domestic samples of laser ceramics is carried out.**

Keywords: *laser ceramics, small-angle scattering spectra, laser heterodyne microprobe analysis, lasing characteristics of ceramics.*

1. Introduction

Laser ceramics is a polycrystalline bulk medium consisting of individual randomly oriented and densely packed crystallites (grains) with irregular boundaries [1–5]. The grains have various size and shape. This can be observed, e.g., in the images of surface sections [4] and bulk cleavages [5] of the ceramics, obtained by means of optical and electron microscopy. The grain sizes lie within the range from a few hundreds of nanometres to a few tens of micrometres, and the mean boundary thickness is from a few units to a few tens of nanometres. The grains of the medium, their boundaries, and the residual pores and cracks in the grains and boundaries, impurity inclusions, and other micro- and submicroinhomogeneities are a source of strong light scattering, both in the process of light propagation through the medium and in the reflection regime. Thus, the laser ceramics is a disperse medium with a variety of different-scale optical inhomogeneities, and, therefore, it is able to scatter light in a wide range of diffraction angles or spatial harmonics, equivalent to them.

The subranges of 'small' and 'large' diffraction angles are most interesting. In the first of them the scattering of the transmitted light is determined mainly by the size of the ceramics grains, while in the second of them the dominant role is played by the grain boundaries, pores, cracks and other microscopic defects of the medium. However, the general feature of these spectra is that they possess an integral character and do not allow determination of spatial position of individual micro- and submicrostructures, scattering light in the medium.

Detailed consideration of the ceramics medium and its noise sources is stimulated by the fact that the scattering noises strongly affect the lasing characteristics of the ceramics. In particular, this is confirmed by the results of Ref. [6], where the influence of the volume density of residual pores on the threshold and differential efficiency of laser oscillation in Nd:YAG ceramics was studied.

Proceeding from the summarised above, the present work was devoted to solving the following problems:

1) Choosing the simplest technique and designing the corresponding hardware and software facilities to measure the energy spectra of scattering in laser ceramics in the region of 'small' (0.5°–6°) diffraction angles. Such spectra are commonly referred to as small-angle ones [7].

2) Developing the laser heterodyne technique for the ceramics microprobe analysis aimed at extracting information about the depth distribution of optical microinhomogeneities. The technique is based on recording the beams of scattered light at 'large' (36°–42°) diffraction angles.

3) Investigating the influence of noise characteristics of the existing samples of ceramics on their lasing properties (oscillation threshold, differential efficiency, etc.).

The experiments aimed at solving the above problems were carried out with the samples of laser Nd:YAG ceramics No. 8 and No. 10 (0.8% Nd, Fryazino Branch of the Institute of Radio Engineering and Electronics, Russian Academy of Sciences) and, for comparison, with the sample of Nd:YAG ceramics R10097 (1% Nd, Baikowski Ltd, Japan).

2. Energy spectra of small-angle scattering

The necessity of studying small-angle light scattering in optical ceramics is caused by a number of reasons. In the region of angles smaller than a few angular degrees a significant increase in the noise spectral density is observed in comparison with the case of scattering (diffraction) in the region of high spatial harmonics of the disperse medium. The level and the character of small-angle light scattering is one of the indicators of the ceramics optical quality, and since the scattering also occurs within the angular divergence of the laser beam, the information about the scattering spectra of the ceramics can be used to estimate the degree of influence of light scattering on the lasing characteristics of the ceramics as an active laser medium. Provided that the character of the dependence of the scattered light spectral intensity on the scattering angle

P.E. Tverdokhleb, Yu.A. Shepetkin, I.Sh. Steinberg, A.Yu. Belikov Institute of Automation and Electrometry, Siberian Branch, Russian Academy of Sciences, prosp. Akad. Koptuga 1, 630090 Novosibirsk, Russia; e-mail: peter@iae.nsk.su, shepetkin@ngs.ru, steinberg@iae.nsk.su, belikov_andrey@ngs.ru;
S.M. Vatnik, I.A. Vedin, P.F. Kurbatov Institute of Laser Physics, Siberian Branch, Russian Academy of Sciences, prosp. Akad. Lavrent'eva 13/3, 630090 Novosibirsk, Russia;
e-mail: vatnik@laser.nsc.ru, vedin@laser.nsc.ru, ion@laser.nsc.ru

Received 3 March 2014; revision received 2 April 2014
Kvantovaya Elektronika **44** (6) 588–593 (2014)
Translated by V.L. Derbov

is known, one can approximately estimate the typical dimensions of the elements (grains) of the scattering medium (ceramics) [7]. In spite of relatively low precision of such an estimate, the results of measuring the scattering spectra obtained by means of one setup can be used for operative comparison of scattering properties of different samples in the process of their manufacturing and use.

The schematic of the developed experimental setup is presented in Fig. 1. The light beam of the He–Ne laser (λ = 0.63 μm, the power 20 mW, the beam spot diameter 1.06 mm at the $1/e^2$ level of maximal intensity) was formed using two iris diaphragms (*2*) and (*3*), intended for attenuating the scattered laser radiation. The direction of light polarisation is parallel to the drawing plane. The direct beam passed through the sample was blocked by the screen (*7*).

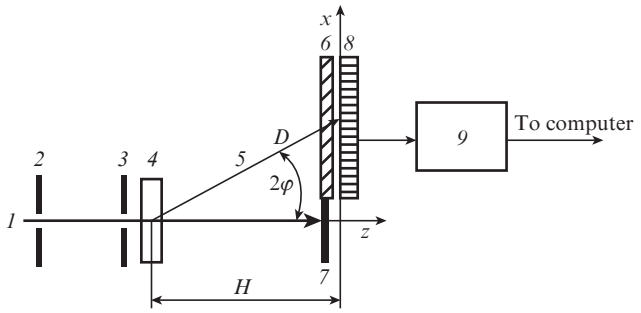

Figure 1. Schematic of the experimental setup for measuring the small-angle scattering spectra: (*1*) laser beam; (*2*, *3*) diaphragms; (*4*) ceramics sample; (*5*) scattered light; (*6*) 1 : 100 optical filter; (*7*) screen; (*8*) photodiode BLPP-369 array; (*9*) photodetector unit (driver) of the array.

The power of scattered light was measured by means of the photodiode array (*8*) and photodetector unit (*9*), which are the structural elements of the multichannel analyser of emission spectra (MAES) [8]. The array has 2580 photodetectors ($\Delta x \times \Delta y$ = 10×1000 μm), arranged with the step δx = 12.5 μm. The photodetector acquisition time is 10 ms, the saturation level is nearly 10^{-12} J, and the dynamic range is 10^4. The neutral optical filter (*6*) is installed in front of the array. The distance between the sample and the array plane is H = 39 cm, and the distance between the scattering centre and the photodetectors is D = 39–39.17 cm. With the above parameters of the scheme elements, the measurement of the small-angle scattering intensity is provided within the angular range $2\varphi = 0.57° - 5.3°$.

The scattering is usually characterised by the spectral density of diffraction efficiency of noise gratings Φ, i.e., the ratio of the noise power P_N/W within the unit band of the 2D spatial frequency W to the power P of light, passed through the sample [9]:

$$\Phi = P_N/WP = P_N\lambda^2D^2/PS = \lambda^2P_N/P\Omega. \quad (1)$$

Here $W = (S\cos^2 2\varphi)/\lambda^2D^2 = \Omega/\lambda^2$; $S = 10^{-2}$ mm^2 is the area of light-sensitive surface of the photodetector (pixel); and Ω is the solid angle of the field of view of a single photodetector. In the case of small-angle scattering $\cos 2\varphi \approx 1$.

If the scattering is axially symmetric with respect to the z axis, then using Eqn (1) we obtain the expression for the total diffraction efficiency η of the scattering within the solid angle, determined by the size of the photodiode array:

$$\eta = \sum_{i=0}^{N-1} \frac{\Phi_i\Omega_i}{\lambda^2} = \sum_{i=0}^{N-1} \frac{\Phi_i 2\pi x_i \delta x}{D_i^2\lambda^2}. \quad (2)$$

Here Φ_i is the value of Φ, obtained using the photodetector with the coordinate x_i, placed at the distance D_i from the scattering centre (Fig. 1), and $\Omega_i = 2\pi x_i\delta x/D_i^2$ is the acceptance solid angle of the scattered radiation within the ring zone, corresponding to this photodetector. In this case it is assumed that within the solid angle Ω_i the quantity Φ_i remains constant.

The dependences of Φ on the spatial frequency of noise gratings $\xi = 2\lambda^{-1}\sin\varphi \approx 2\lambda^{-1}\varphi$, measured in three samples of ceramics are presented in Fig. 2. The characteristics were obtained after the smoothing (using the least-squares method) of the noises, caused by the speckle structure of the scattered light.

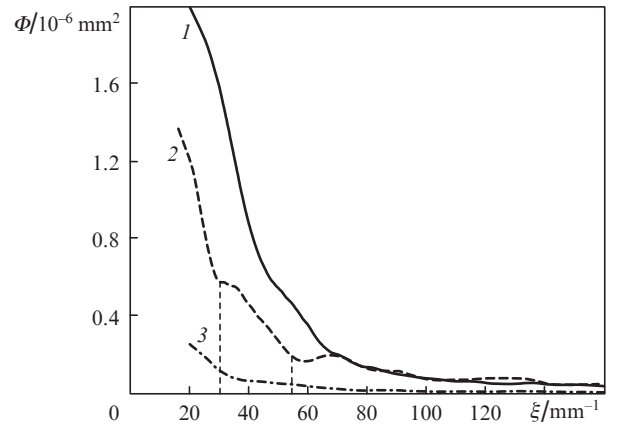

Figure 2. Energy spectra of scattering from the ceramics samples No. 10 (*1*), No. 8 (*2*), and R10097 (*3*).

In the absence of ceramics the spectral density Φ varied from 5.1×10^{-8} mm^2 at $\xi \approx 20$ mm^{-1} to 1.4×10^{-9} mm^2 at $\xi \approx 160$ mm^{-1}. These values of Φ were subtracted from the results of measuring the ceramics scattering noise.

To estimate the typical scatterer size we use the Guignet formula [7], i.e., consider the dependence of the noise intensity $I_N = P_N/S$ on the square of the circular spatial frequency of noise gratings $q^2 = (2\pi\xi)^2 \approx (4\pi\lambda^{-1}\varphi)^2$:

$$I_N(q) \approx I_N(0)\exp(-q^2R_g^2/3) \text{ при } q \to 0, \quad (3)$$

where R_g is the radius of inertia for the scattering particle.

From Eqn (3) follows that the greater is the characteristic inhomogeneity size, the steeper falls the normalised dependence $I_N^*(\xi) = I_N(\xi)/I_N(\xi_{in})$ with the growth of spatial frequency, where ξ_{in} = 20 mm^{-1} is the initial value of ξ. Such dependences for the samples of ceramics under study are presented in Fig. 3. One can see that the grain size R_g is nearly the same in all samples.

To estimate the characteristic size of inhomogeneities (grains) we use the technique, presented in Ref. [10]. Thus, it follows from Eqn (1) that $\Phi \propto I_N$, and therefore the Guinier formula can be presented in the form

$$\Phi(q) \approx \Phi(0)\exp(-q^2R_g^2/3), \quad (4)$$

or, after taking the logarithm,

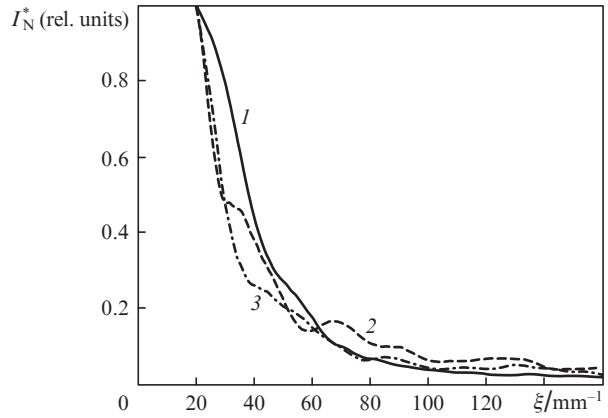

Figure 3. Dependences of the normalised intensity of the scattered light on the spatial frequency of noise gratings for samples No. 10 (*1*), No. 8 (*2*), and R10097 (*3*).

$$\ln[\Phi(q)] = \ln[\Phi(0)] - q^2R_g^2/3. \quad (5)$$

Then, in the plot of the function $\ln[\Phi(q)]$ the regions are selected in which the dependence $\ln[\Phi(q)]$ on q^2 is approximately linear [10]. As an example, the boundaries of such regions for curve (*2*) in Fig. 2 are marked by dashes. In each region the linear regression function is found, which has the form $R(v) = a + bv$, where $v = q^2$. This function approximates the counts of the initial data $\ln[\Phi(q)]$ to $R(v)$ with the smallest mean square error. For each region the validity coefficient of the approximation is determines using the formula [10]

$$Q^2 = 1 - \sum_{i=1}^{k}(y_i - f_i)^2 / \sum_{i=1}^{k}(y_i - \bar{y})^2, \quad (6)$$

where k is the number of counts within the chosen region; y_i are the experimental values of the function $\ln[\Phi(q)]$; $\bar{y}$ is their arithmetical mean value; and f_i are the values of the approximation function within this region.

The validity coefficients should be as close to 1, as possible; therefore, if necessary, the boundaries of the region can be defined more exactly and the approximation process is repeated.

We present the results of the approximation in the form (4), where $\Phi(0) = \exp(a)$, $R_g = (-3b)^{1/2}$. The results of the experimental data processing are presented in Table 1. Here the values of the total diffraction efficiency η, obtained from Eqn (2), are also presented.

In Ref. [7] the formulae that relate the inertia radius R_g to the dimensions of simple geometric bodies are presented. In the first approximation the characteristic shape of the grain boundary can be assumed to be a polyhedral prism [4]. The side surface of such a prism is close to the surface of a thin-walled cylinder, the radius R of which equals the radius of the circle, circumscribing the polygon, $R = d/2 \approx R_g$, where d is the characteristic size of the grain.

3. Determination of depth distribution of optical inhomogeneities in ceramics using the laser heterodyne microprobe analysis

The essence of the proposed method of laser heterodyne microprobe analysis [11] will be explained by means of Fig. 4. Here we use two coherent focused light beams, the reference one, (*1*), and the heterodyne one, (*2*). The heterodyne beam frequency is shifted with respect to the frequency of the reference beam by $\Delta F = 88$ MHz. Within the volume, where the beams overlap, a moving interference micrograting is formed, which overlaps with the noise 'grating' (*4*) inside the sample of the laser ceramics (*3*). The light beam (*5*) arises as a result of diffraction of the beam (*2*) at the noise grating (*4*). If the spatial frequency of the noise grating is equal to the spatial frequency of the moving micrograting or close to it, then the beam (*5*) will propagate in the same direction (collinearly) as the beam (*1*). The interaction of two collinear beams of light

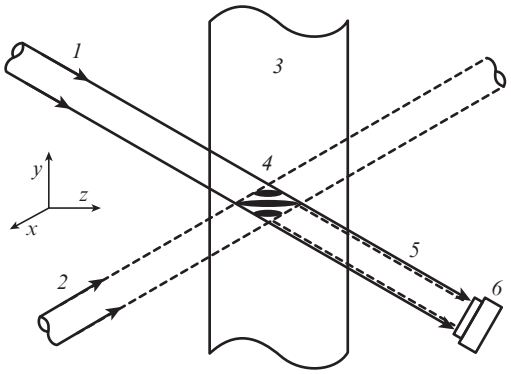

Figure 4. Schematic diagram for studying the spatial distribution of the optical inhomogeneities in a bulk material using the collinear heterodyne detection: (*1*) reference beam; (*2*) heterodyne beam; (*3*) laser ceramics; (*4*) noise 'grating'; (*5*) beam, arising as a result of diffraction; (*6*) photodetector.

Table 1. Characteristics of the ceramics samples, obtained as a result of processing the small-angle light scattering spectra.

Sample	Number of the approximation zone	ξ/μm^{-1}	$\Phi(0)$/μm^2	R_g/μm	Q^2	η/10x^{-3}
No 8	1	16–30	2.1	11	0.980	7.5
	2	30–54	1.8	7.1	0.990	
	3	54–147	0.21	2.4	0.850	
No 10	1	20–47.4	3	7.7	0.991	10
	2	47.4–67.6	1.9	6.2	0.991	
	3	67.6–142	0.19	2.5	0.853	
R10097	1	20–36.6	0.46	10.4	0.993	1.4
	2	36.6–69.5	0.112	4.8	0.993	
	3	69.5–161	0.022	1.73	0.746	

with different frequencies gives rise to a photocurrent with the difference frequency ΔF at the output of the photodetector (*6*). This signal carries information about the amplitude of the noise grating, and the photodiode (*6*) detects only the light field of the heterodyne beam, scattered by the grating, which has the same direction (angular spectrum of spatial harmonics) as the part of the reference beam (*1*) that passes without diffraction.

The detection of optical inhomogeneities in other microvolumes of the ceramics is implemented by a high-precision displacements of the sample along the axes x, y, and z with respect to the focused beams crossing. The range of possible displacement with the used piezoelectric positioner is equal to 310 μm, which, with the ceramics refractive index $n = 1.8$ taken into account, restricts the range of depth scanning to 558 μm.

It should be noted that the heterodyne detection occurs only in the overlap region of the beams (*1*) and (*2*). Therefore, the noises related to the scattering at the surface and in other regions of the ceramics do not affect the result of detection.

The complete scheme of the experimental setup and the principle of its operation do not differ from the earlier reported prototype [12]. As a source of radiation we used a semiconductor laser with the wavelength of 660 nm, and the beam focusing was implemented using the microscope objective with the magnification of 40, the focal length of 4.5 mm, the flange focal distance of 2 mm, and the numerical aperture NA = 0.6. With these parameters in the focal plane of the microscope objective the micrograting was formed with the size of $\Delta x \times \Delta y = 0.8 \times 1.3$ μm. The shift of the radiation frequency in the heterodyne beam was introduced using an acousto-optic light modulator.

The spatial frequency of the micrograting, formed in the ceramics medium, is determined by the expression $\xi_0 = 2\sin\theta/\lambda$, where λ is the laser radiation wavelength, and θ is a half of the angle between the light beam axes outside the medium. Thus, for $\theta = 20°$, $\lambda = 0.66$ μm the spatial frequency of the grating amounts to 1040 mm^{-1}. Keeping in mind that the micrograting formation is implemented by means of focused Gaussian beams the range of spatial harmonics of such microgratings can be estimated to lie within 706–1346 mm^{-1} at the amplitude half-maximum level. The tuning bandwidth for the central spatial frequency ξ_0 of the microgratings is not large. It lies within the range 900–1100 mm^{-1} and is determined by the characteristics of the used acoustooptical modulator (AOM) and the parameters of the optical system of heterodyne microprobe analysis. The thickness of the grating (at the intensity half-maximum level) for diffraction-limited beams is equal to $\Delta z = 2r_{0y}n/\sin\theta$, where $2r_{0y}$ is the y-axis size of the focused Gaussian beam waist. Thus, for $r_{0y} = 0.65$ μm, $n = 1.8$, $\theta = 20°$, $\lambda = 0.66$ μm we get $\Delta z = 8.8$ μm. The thickness of the spatial selection region, measured at the depth of 20 μm, amounts to $\Delta z = 7.2$ μm, which characterises the depth resolution capability of the technique, close to the diffraction limit (6.8 μm). Taking the above values of the micrograting size along the axes x and y into account, we get the minimal size of the probing micrograting in the ceramics to be $\Delta x \times \Delta y \times \Delta z = 0.8 \times 1.3 \times 7.2$ μm. However, when moving the light probe deeper into the sample, the size of the focused beam increases due to spherical aberration, which leads to worse resolution of the present method. Thus, at the depth of 500 μm the measured size of the micrograting is equal to $\Delta x \times \Delta y \times \Delta z = 1.2 \times 1.9 \times 15.3$ μm.

It is worth noting that at the above values of the micrograting spatial frequency and its lateral dimensions the maximal signal of the heterodyne microprobe will be observed when the transverse size of the optical inhomogeneities are equal to nearly 1–3 μm. This may be the ceramics sample grains themselves, possessing the appropriate size, or the boundaries of larger grains (exceeding 5 μm).

The diffraction efficiency of microgratings in collinear heterodyne detection was determined in the following way. As mentioned above, two collinear light beams hit the photodiode. One of them is the heterodyne one, diffracted preliminarily at the AOM (possessing a frequency shift) and then at the micrograting. The second beam is the reference one, passing the AOM without diffraction. At the output of the photodiode the alternating current is generated. Its frequency is equal to the difference of the frequencies of the light beams, and its amplitude is

$$i_{\text{res}} = 2(i_{\text{get}} i_{\text{ref}})^{1/2}, \tag{7}$$

where i_{get} and i_{ref} are the photocurrents, obtained separately from the heterodyne and the reference beam. Assuming the diffraction efficiency of the AOM to be 50%, and the photocurrent value at the modulator switched off to be i_0, we obtain $i_{\text{get}} = \eta i_0/2$, $i_{\text{ref}} = i_0/2$. Substituting the expressions for i_{get} and i_{ref} into Eqn (7), we get $\eta = (i_{\text{res}}/i_0)^2$. Assuming the noise micrograting to be mainly a phase one, the amplitude of modulation of the refractive index Δn can be found using the known Kogelnik formula [13] for phase transmission holograms.

The object of our study was sample No. 8 of laser Nd:YAG ceramics (0.8% Nd), having the shape of a disk with the diameter 15.6 mm and the thickness 3.2 mm. Figure 5 shows the character of the response variation, i.e., the signal at the output of the photodetector (*6*) (see Fig. 5), measured under the displacement of the double-beam laser probe along the sample thickness. The results of scanning are obtained within one of the regions near the sample centre. The abscissa axis shows the depth of penetration of the laser probe into the medium in micrometres. The region from zero to 50 μm along the z axis corresponds to air, and the region from 50 to 500 μm corresponds to the ceramics. The mean square value of the read-out signal amplitude in air amounted to $U_{\text{sc}} = 4.9$ mV. It is determined by the scattering by the optical elements in the region of light beams intersection, by the noises of the photocurrent amplifier, and by the noise pickup in the elements of electronic circuits. The mean square value of the read-out signal from the ceramics (depth from 50 to 500 μm) amounts to

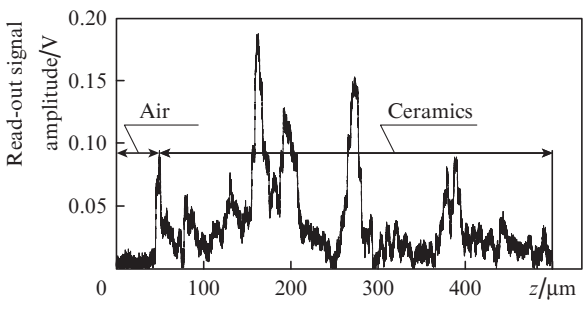

Figure 5. Amplitude of the read-out signal from the depth-scanned (z axis) ceramics sample.

33 mV. The modulation amplitude of the refractive index, corresponding to this value, is nearly 2×10^{-5}. The peak value of the read-out signal in the ceramics amounted to 170 mV (Fig. 5), and the modulation amplitude of the refractive index was equal to $\sim10^{-4}$.

A more complete presentation of the distribution of optical inhomogeneities is given by the 2D picture, obtained as a result of 31 cycles of depth scanning (along the z axis) and sequential shift by 2 μm in the lateral direction (along the y axis). Figure 6a presents an example of a synthesised image (topogram), obtained in the course of such scanning. The presented picture is the image of the 2D distribution of the response, which in turn is a convolution of the read-out micrograting and the noise grating. In this connection the size of the optical inhomogeneity in Fig. 6a can be evaluated as $\Delta y\times\Delta z = 2.2\times13$ μm. One can suppose that if the observed depth size of the inhomogeneity is greater than 7–10 μm, than it most probably corresponds to the response to a few grains placed in turn, each having the size smaller than the depth size of the instrumental function. Three-dimensional presentation of the distribution of optical inhomogeneities in the ceramics medium could be much more informative. We plan to obtain such images in the future. The question of the nature and structure of optical inhomogeneities, observed in the course of depth probing of laser ceramics, is still open for discussion and requires additional studies.

At present it is possible to state only that such inhomogeneities are not pores in the laser ceramics, since the difference of refraction indices at the pore boundaries amounts to ~0.8, and the amplitude of the read-out signal in this case would be by 4 orders of magnitude higher than the observed value.

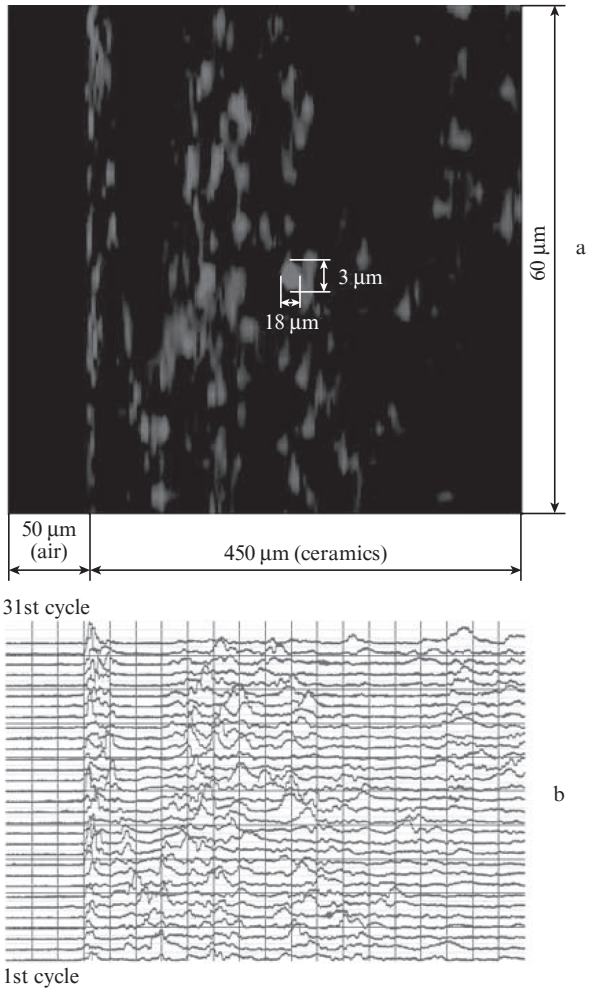

Figure 6. Graphic representation of the 2D scanning results of the laser ceramics: (a) read-out signal topogram from the 60×450 μm region (the scale is different for the axes y and z), and (b) the read-out signal amplitudes, recorded in all (from the 1st to 31st) scanning cycles.

4. Evaluating the influence of scattering on the lasing characteristics of the ceramics

The lasing characteristics of the laser Nd : YAG ceramics were studied in the geometry of a short linear cavity (the physical length $L = 20$ mm); the experimental technique it thoroughly described in Refs [1, 14]. After deep polishing, the planar surfaces of samples No. 8 and No. 10 (disks ⌀15.6×3.2 mm, 0.8% ND) and reference sample R10097 (disk ⌀10×2.5 mm, 1% Nd) were covered with dielectric coatings. The broadband antireflection coating had the residual reflection smaller than 0.15% at the pump (808 nm) and lasing (1064 nm) wavelengths. The combined reflecting coating, consisting of the dielectric highly reflecting mirror (with the reflection coefficient exceeding 99.8% at $\lambda = 1064$ nm) and the additional metallised layer that provided a high reflection coefficient for the pump radiation at the incidence angles 0–30°. For efficient heat removal the ceramics disks were mounted on the copper heatsinks with the indium 100 μm thick foil spacer between them, using various methods of soldering and pressing. The pumping of all ceramics samples was implemented with the collimated radiation of two diode arrays with the total power up to ~50 W, the pump beam spot diameter in the focal plane amounted to 0.95 mm. The laser cavity was formed by an external concave mirror and a planar mirror at the active element from the side of the heatsink. The output coupler was a concave spherical one with the radius $r = -40$ mm and the transmission coefficient $T = 3\%$ at the wavelength $\lambda = 1064$ nm. Since the metallisation of the rear mirror on samples No. 8 and No. 10 had very low adhesion, the measurements of the oscillation parameters were carried out in the regime of quasicontinuous pumping with the duty cycle 14% (7 ms/50 ms) with the maximal value of the pump radiation power 25 W.

The results of the lasing experiments are presented in Fig. 7. The differential efficiencies and oscillation thresholds amounted to (according to linear approximation) 44.7% and 1.0 W (R10097), 20.8% and 1.7 W (No. 10), 9.5% and 4.3 W (No. 8).

The results of the study of optical inhomogeneities in the ceramics samples, obtained using the method of heterodyne microprobe analysis, are presented in Fig. 8. The comparison of the data in Figs 7 and 8 demonstrates the presence of correlation between the lasing characteristics and the distribution of optical inhomogeneities. The qualitative pictures of the optical inhomogeneity distributions can be completed by the results of measuring the spectral density of the diffraction efficiency Φ of the noise gratings in the ceramics samples. Thus, within the spatial frequency range 994–1147 mm^{-1} it amounts to 4.84×10^{-9} mm^2 for sample No. 10, 6.4×10^{-9} mm^2 for sample No. 8, and $(3.7–21)\times10^{-10}$ mm^2 for sample R10097. The latter sample has plane-parallel opposite faces, and the level of scattering depends on the small variation of the incidence angle of the probe light beam. As it could be expected, the best lasing parameters (the oscillation threshold and the differential efficiency) were found in the sample of ceramics R10097, where the inhomogeneities are practically

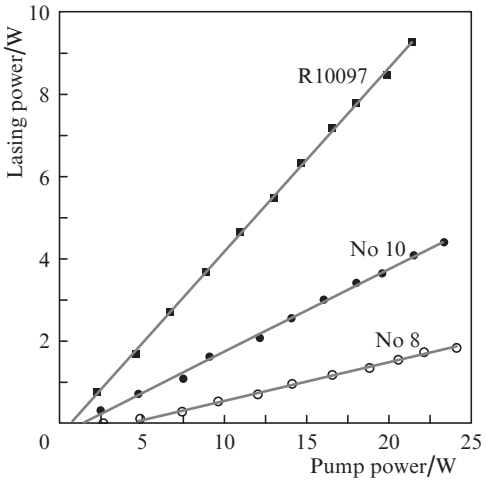

Figure 7. Lasing characteristics of the studied samples of the Nd:YAG ceramics with the differential efficiency 44.7% (R10097), 20.8% (No. 10), 9.5% (No. 8).

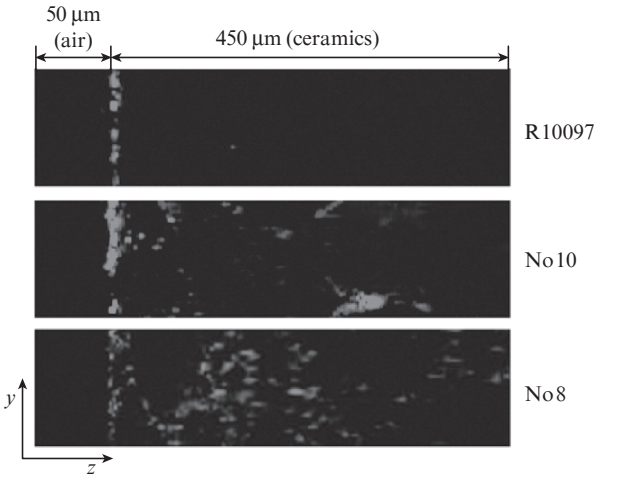

Figure 8. Read-out signal topograms for three samples of laser ceramics. The dimension of the studies region is 60×450 μm.

absent and, therefore, the scattering is minimal. Integrally, besides the optical losses, the threshold and efficiency of oscillation will be affected by the degree of microstructure optical homogeneity of the ceramics, which should be sufficient to provide the phase coherence conditions. At present it seems apparent that both the magnitude of the optical losses (including the small-angle ones), and the small-scale inhomogeneity of the refractive index, leading to random phase incursions, are determined by the whole set of microstructure defects within the ceramics volume, and for revealing the additional mutual correlations between these parameters it could be reasonable to perform direct measurements of losses at the wavelength of the laser radiation, as well as determine the coefficients of unsaturated gain of the ceramics depending on the absorbed pump power.

5. Conclusions

The major results of the performed study can be summarised as follows.

The energy spectra of small-angle (0.5°–6°) light scattering are measured in the disperse media of domestic (0.8% Nd, No. 8 and No. 10) and foreign (1% Nd, R10097) samples of laser ceramics. Based on these data it is established that the characteristic size of grains lie within the range 3–22 μm. It is shown that the scattering efficiency for the R10097 sample is nearly 5–8 times lower than in the domestic samples. The presence of three regions in the Guinier dependences, two of them providing the linear approximation with the validity ~0.99, allows the assumption that the grain sizes in the studied samples of the ceramics R10097 and No. 8 are distributed in correspondence with the three-modal function law, however, this assumption requires further verification.

The laser technique of depth-resolved heterodyne microprobe analysis of laser ceramics is proposed and introduced into the experimental practice. The technique implies the measurement of the scattered light intensity at large (36°–42°) diffraction angles. The size of the light probe inside the ceramics volume is $\Delta x \times \Delta y \times \Delta z = 0.8 \times 1.3 \times 6.8$ μm. The 2D microimages of the ceramics thickness-resolved refractive index fluctuations are obtained experimentally (the modulation amplitude at the level of 10^{-4}). The size of the scanning zone is 60×450 μm. The dependence of lasing characteristics (oscillation threshold, differential efficiency) upon the presence and 'concentration' of such optical inhomogeneities is revealed. It is shown that the best lasing parameters are present in sample R0097, where the depth-distributed fluctuations of the refractive index are practically absent.

Acknowledgements. The work was supported by the Presidium of the Russian Academy of Sciences (Extreme Light Fields and Their Applications Programme) and the Russian Foundation for Basic Research (Grant No. 14-02-00732-a).

References

1. Bagayev S.N., Osipov V.V., Ivanov M.G., Solomonov V.I., Platonov V.V., Orlov A.N., Rasuleva A.V., Ivanov V.V., Kaygorodov A.V., Vatnik S.M., Vedin I.F., Mayorov A.P., Pestryakov E.V., Shestakov A.V., Salkov A.V. *Kvantovaya Elektron*., **38** (9), 840 (2008) [*Quantum Electron*., **38** (9), 840 (2008)].
2. Garanin S.G., Rukavishnikov N.N., Dmitryuk A.V., Zhilin A.A., Mikhaylov M.D. *Opt. Zh*., **77** (9), 52 (2010) [*Journal of Optical Technology*, **77** (9), 565 (2010)].
3. Garanin S.G., Dmitryuk A.V., Mikhaylov M.D., Zhilin A.A., Rukavishnikov N.N. *Opt. Zh*., **78** (6), 60 (2011) [*Journal of Optical Technology*, **78** (6), 393 (2011)].
4. Balabanov S.S., Bykov Yu.V., Egorov S.V., et al. *Kvantovaya Elektron*., **43** (4), 396 (2013) [*Quantum Electron*., **43** (4), 396 (2013)].
5. Kaminskii A.A., Taranov A.V., Khazanov E.N. *Kvantovaya Elektron.*, **43** (3), 282 (2013) [*Quantum Electron*., **43** (3), 282 (2013)].
6. Ikesue A., Yoshida K. *J. Mater. Sci.*, **34** (6), 1189 (1999).
7. Svergun D.I., Feigin L.A. *Rentgenovskoye i neitronnoye malouglovoye rasseyaniye* (X-ray and Neutron Small-Angle Scattering) (Moscow: Nauka, 1986).
8. Labusov V.A., Garanin V.G., Shelpakova I.R. *Zh. Analit. Khim*., **67**, 697 (2012) [*Journal of Analytical Chemistry*, **67**, 632 (2012)].
9. Collier R.J., Burckhardt C.B., Lin L.H. *Optical Holography* (New York/London: Academic Press, 1971).
10. Bunkin N.F., Suyazov N.V., Tsipenyuk D.Yu. *Kvantovaya Elektron.*, **35** (2), 180 (2005) [*Quantum Electron*., **35** (2), 180 (2005)].
11. Rudakov I.B., Shteinberg I.Sh., Schepetkin Yu.A. *Avtometriya*, (3), 76 (1991).
12. Belikov A.Yu., Vyukhina N.N., Zatolokin V.N., Tverdokhleb P.E., Trubetskoy A.V., Shteinberg I.Sh., Schepetkin Yu.A. *Avtometriya*, **43** (1), 76 (2007) [*Optoelectronics, Instrumentation and Data Processing*, **43** (1), 59 (2007)].
13. Kogelnik H. *Bell Syst. Tech. J.*, **48**, 2909 (1969).
14. Vatnik S.M., Osipov V.V., Vedin I.A., Kurbatov P.F. *Kvantovaya Elektron*., **43** (3), 288 (2013) [*Quantum Electron*., **43** (3), 288 (2013)].